Conductivity Studies of Nanostructured TiO_2 Films Permeated with Electrolyte

Helena Greijer Agrell, Gerrit Boschloo,* and Anders Hagfeldt

Department of Physical Chemistry, P. O. Box 579, Uppsala University, 751 23 Uppsala, Sweden

Received: October 15, 2003; In Final Form: June 1, 2004

Charge transport in nanostructured TiO_2 films permeated with an electrolyte was studied, using temperature-dependent conductivity and electron accumulation measurements. Two regions for charge transport were distinguished from the relationship between conductivity and electron concentration. In the first region (∼1−20 electrons per TiO_2 particle), the effective electron mobility is dependent on the electron concentration and values between 7×10^{-4} and 78×10^{-4} $cm^2\ V^{-1}\ s^{-1}$ were determined. The activation energy of the mobility was ∼0.3 eV. The charge transport can be described with a trapping/detrapping model that involves localized band-gap states. In the second region (> 20 electrons per TiO_2 particle), the effective electron mobility is independent of electron concentration and values of $\sim 150 \times 10^{-4}$ $cm^2\ V^{-1}\ s^{-1}$ are calculated. The activation energy of mobility is in the range of 0−0.15 eV, depending on the electrolyte. Transport of electrons in the conduction band seems to be the most applicable model.

1. Introduction

Nanostructured TiO_2 films are the basis of dye-sensitized nanostructured solar cells[1] but also find applications in light-emitting diodes, electrochromics, photocatalysis, biosensors, and batteries. The charge-transport properties in such films remain to be elucidated, and the details regarding the transport mechanisms are not fully understood.[2,3] Some techniques used to study transport properties are photocurrent transients,[4] intensity-modulated photocurrent spectroscopy,[5−10] and impedance spectroscopy.[11,12] Optimization of the electron transport in nanostructured TiO_2 is essential for dye-sensitized cells, to minimize recombination losses during transport due to the reaction of electrons with the redox species in the electrolyte.

Electron transport in nanostructured semiconductor films is assumed to proceed primarily via diffusion, because of the absence of a significant electrical potential gradient in the film. On the microscopic (or local) level, an electrical potential decrease occurs across the Helmholtz layer at the TiO_2/electrolyte interface. On the macroscopic level, no significant electrical potential decrease exists within the porous TiO_2 when it is in contact with an electrolyte. A driving force for the electron flow, through the porous structure toward the conducting substrate, may be the equilibration of the electron density through the film. The properties of charge transport are often explained by considering the involvement of electron trapping in surface states. The mechanism is most often discussed in terms of a trapping/detrapping model, where electrons move between band-gap states via the conduction band. Alternatively, a hopping model can be used, where the electron moves between localized band-gap states.[3]

Nanostructured anatase TiO_2 is believed to have a high density of surface traps. Electrons trapped in surface states of nanostructured TiO_2 have been observed earlier using spectroelectrochemical methods.[13] The density was determined to 12 electrons trapped per TiO_2 particle, with an energetic position of ∼0.5 eV below the conduction band edge. The pH dependency of the deep trap density indicates that deep traps are surface-related.[14] The diffusion coefficient of photogenerated electrons in nanostructured TiO_2 films has been shown to be dependent on light intensity and ion concentration in the electrolyte. Diffusion coefficients in the ranges of 10^{-6}−10^{-4} cm^2/s,[4,15,16] and 10^{-8}−10^{-5} cm^2/s,[5] have been determined, depending on light intensity (I_0). From intensity-modulated photocurrent spectroscopy studies of the dye-sensitized solar cell under "normal" operating conditions, it was suggested that the majority of electrons is trapped in localized levels below the conduction band from which they can escape (detrapping) by thermal activation.[5,7,9] The observed intensity dependence of the diffusion coefficient can be explained by the upward movement of the quasi-Fermi level through the distribution of shallow traps. The average electron occupancy in a dye-sensitized solar cell under open-circuit conditions at an incident flux of 1.4×10^{16} cm^{-2} (39 W/m^2) was estimated to be close to two electrons per TiO_2 particle.[17] The average concentration of conduction band electrons seemed to saturate at one electron per particle in a dye-sensitized solar cell under short-circuit conditions, irrespective of the irradiation intensity (0.7−330 W/m^2).[8] The effective diffusion coefficient at a photon flux of 10^{16} cm^2/s is $\sim 10^{-5}$ cm^2/s.[5] In comparison, the diffusion coefficient of free electrons in the conduction band is on the order of 10^{-2} cm^2/s for bulk anatase.[18]

One natural direction to explore the charge-transport properties would be to perform conductivity measurements; however, relatively few studies have been reported so far. The conductivity and its dependence of charge carrier concentration of nanostructured ZnO[19] and TiO_2 films[20] permeated with electrolytes was obtained from resistance and electron accumulation measurements with a method developed earlier.[21] Two inert electrodes are separated by a small gap, which is filled by the material to be studied. By connecting them to the working electrode inputs of a bipotentiostat in a standard electrochemical cell setup, one can individually control the electrochemical potentials of both electrodes and the electron concentration in the film. The resistance of the TiO_2 film can be determined from measuring the current through the film (Figure 1) when a

* Author to whom correspondence should be addressed. E-mail: gerrit.boschloo@fki.uu.se.

10.1021/jp037119p CCC: $27.50 © 2004 American Chemical Society
Published on Web 07/27/2004

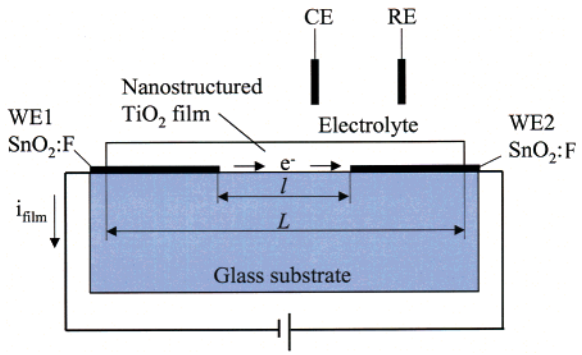

Figure 1. Schematic picture of the electrode geometry used in the resistance measurement. Fluorine-doped SnO_2, separated by a small gap ($l = 90$ μm) and filled with a nanostructured TiO_2 film (with length L), formed the working electrodes (WE1 and WE2). When a small potential difference is applied between WE1 and WE2, a current (i_{film}) will flow between the two working electrodes.

small potential difference is applied between the electrodes. The electron mobility in the system is obtained from the relation between conductivity and electron concentration. Electron drift mobilities in nanostructured TiO_2 films were determined to be $5 \times 10^{-3}-50 \times 10^{-3}$ cm^2 V^{-1} s^{-1}, depending on Li^+ insertion effects[20] and in nanostructured ZnO were determined to be $10^{-3}-10^{-1}$ cm^2 V^{-1} s^{-1}, depending on electron density ($5 \times 10^{18}-1 \times 10^{20}$ cm^{-3}).[19] For the nanostructured ZnO, the mobility was not dependent on the type and concentration of the inert electrolyte ions.

In this work, the temperature and potential dependence of conductivity and electron accumulation was studied in nanostructured TiO_2 that was permeated with an electrolyte. Also, the concentration and nature of the electrolyte was varied. Based on the results and the determined activation energies of electron conduction, mobility, and accumulation, the mechanism of electron transport in such films will be discussed.

2. Experimental Section

2.1. Preparation of Samples. Nanostructured TiO_2 (anatase) samples were prepared from a colloidal TiO_2 solution. The TiO_2 colloidal solution was prepared via the hydrolysis of titanium tetraisopropoxide.[1] The TiO_2 solution was spread onto transparent conducting glass sheets (Pilkington TEC8, fluorine-doped SnO_2 glass with a sheet resistance of 8 Ω/square) with a laser-scribed gap of 90 μm (l in Figure 1). Laser Nova AB in Östersund, Sweden, performed the laser scribing. To remove residual SnO_2 from the laser-scribed gap, the conducting glass sheets were chemically etched in 0.1 M HCl containing zinc metal pieces, followed by careful rinsing with water and ethanol before the TiO_2 solution was applied. Using adhesive tape (Scotch Magic, 3M) as a frame and spacer, a thin film was formed by raking off the excess colloidal solution with a glass rod. The samples were heated in air at 450 °C for 20 min to sinter the particles. The size of the TiO_2 particles was 10−14 nm in the resulting nanostructured electrode. To minimize unwanted reactions at the interface between the SnO_2 surface and the electrolyte, areas of bare SnO_2 surface that would contact the electrolyte were isolated from the electrode by mechanical scribing. Just before the samples were transferred into an argon atmosphere glovebox, they were heated again for 10 min at 450 °C to remove any adsorbed water. In later experiments, the mechanical scribing procedure was replaced by the application of a layer of epoxy on the bare SnO_2, which was done in the glovebox.

2.2. Electrochemical Experiments. The sample was immersed in an electrolyte solution during the measurements. The solutions used were as follows: 10 mM, 100 mM, and 500 mM lithium trifluoromethanesulfonate ($LiCF_3SO_3$); 500 mM $LiCF_3SO_3$ and 500 mM 4-*tert*-butylpyridine (4TBP); and 10 mM cesium perchlorate ($CsClO_4$) in propylene carbonate (PC). A schematic picture of the electrode geometry and the experimental setup is shown in Figure 1. The measurements were performed in a standard electrochemical cell. Fluorine-doped SnO_2 (SnO_2:F) that was separated by a small gap ($l = 90$ um) and covered with a nanostructured TiO_2 film formed the two working electrodes (WE1 and WE2). A platinum wire served as the counter electrode. Ag/AgCl with saturated LiCl in ethanol was used as the reference electrode when the salt $LiCF_3SO_3$ in propylene carbonate was used; Ag/Ag^+ with 2 mM $AgNO_3$ and 10 mM $CsClO_4$ in propylene carbonate was used as the reference electrode for the salt $CsClO_4$. All potentials mentioned are relative to the reference electrode Ag/AgCl with saturated LiCl in ethanol (+140 mV vs NHE). An Autolab Ecochemie bipotentiostat (PGstat 10) provided separate potential control and current monitoring of WE1 and WE2. The electrolyte vessel was mounted in a metallic mantle, surrounded by tubular heating elements. A thermostat (Lauda Ecoline RE106) controlled the temperature of the heat medium within the tubular elements. Experiments were performed in the temperature range of 15−55 °C. No correction is made for the temperature dependence of the reference electrode. The potential of a Ag/AgCl reference electrode with saturated KCl in ethanol changes 40 mV in this temperature range. A similar change is expected for the case of LiCl. All measurements were performed in darkness in an argon atmosphere glovebox.

The conductivity and electron accumulation measurements at different potentials and temperatures in this study are based on three actions, in the following order: charge accumulation, resistance experiments, and charge extraction. During accumulation, electrons flow from the SnO_2:F substrate into the nanostructured TiO_2. This negative charge will be charge-compensated by a positive ionic charge in the electrolyte inside the porous nanostructure: cations will move in and anions will move out. The amount of accumulated electronic charge in the TiO_2 film was determined from a potential step measurement by current integration (chronoamperometry). During the potential step measurements, WE1 and WE2 were connected together and used as a single working electrode. To empty the TiO_2 film from electrons, a potential of +0.5 V was first applied for 1 min. The potential of interest (U_a) then was applied for 2 min. In the resistance experiment, WE1 and WE2 were first held at the U_a value for 2 min and then a small potential step ($\Delta U = -10$ mV) was applied to WE1. The change in equilibrium current at WE1 and WE2 (Δi_1 and Δi_2, respectively) was measured after 1 min. Longer waiting times did not change the measured current. The measured equilibrium current remained within a deviation of 1% during the last 10 s (up to 6% at the most-positive potentials of −0.5 V and −0.6 V). In the extraction of electrons, a potential step measurement was applied from U_a (1 min) to +0.5 V (2 min). The accumulated charge (Q_{acc}) and extracted charge (Q_{ext}) differed slightly ($0.8 < Q_{acc}/Q_{ext} < 1.2$). In the potential range that was investigated, no intercalation of Li^+ ions or any other Faradaic reactions were observed.

2.3. Control Experiments. The current−potential characteristics were studied for electrodes with and without the TiO_2 films. The fluorine-doped SnO_2 on both sides of the gap were connected. Figure 2 shows cyclic voltammograms for the two

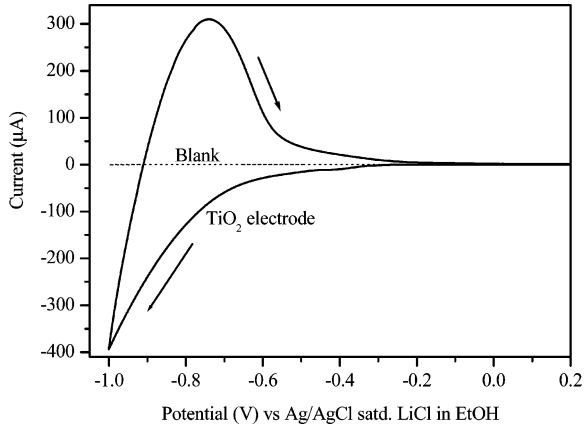

Figure 2. Cyclic voltammograms of two laser-scribed electrodes: TiO_2/SnO_2:F/glass and bare SnO_2(F)/glass being a blank, permeated with the electrolyte 500 mM $LiCF_3SO_3$ in propylene carbonate. Arrows indicate the scan direction. The sweep started at a potential of +0.5 V. Scan rate was 10 mV/s.

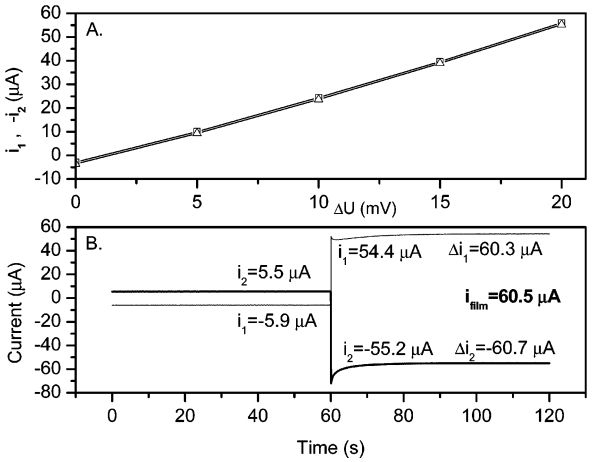

Figure 3. (A) Measured equilibrium current at working electrodes 1 and 2 of the nanostructured TiO_2 film permeated with the electrolyte 500 mM $LiCF_3SO_3$ in propylene carbonate, as a function of their potential difference (ΔU). The applied potentials were −0.700, −0.705, −0.710, −0.715, and −0.720 V at WE1 and −0.700 V at WE2 (versus Ag/AgCl with saturated LiCl in ethanol). The equilibrium current at working electrodes 1 and 2 was measured 2 min after application of the potential difference. (B) Example of the current traces during a conductivity experiment. Initially, $U_1 = U_2 = -0.80$ V. At $t = 60$ s U_1 is stepped to −0.81 V. Measured equilibrium currents are indicated.

electrodes TiO_2/SnO_2:F and bare SnO_2:F being a blank in 500 mM $LiCF_3SO_3$. As seen in Figure 2, the charging currents of the SnO_2:F and possible leak currents between the SnO_2:F and the electrolyte are negligible in this setup, in comparison to the currents through the TiO_2 film.

2.4. Resistance of TiO_2 Film Permeated with Electrolyte. The current in the working electrode of a bare laser-scribed glass sheet was negligible when a potential difference (20 mV) was applied over the gap. Thus, leak currents both through possible residues of SnO_2:F (after the laser scribing) in the gap region and through the electrolyte were negligible in the resistance experiments. The equilibrium current at WE1 and WE2 (i_1 and i_2) at a potential difference of $\Delta U = 0-20$ mV over a TiO_2 film is presented in Figure 3A. The absolute values of the equilibrium current were almost equal. In other words, the Faradaic currents through the electrodes were negligibly small.[19] The equilibrium current through the TiO_2 film was invariably proportional to the applied potential difference over the TiO_2 film. When $\Delta U = 0$, there is still a current flow between WE1 and WE2, because of a small error in the bipotentiostat output. Therefore, Δi_1 and Δi_2 are used to calculate the current through the nanostructured film (i_{film}) that is caused by ΔU, $i_{film} = (\Delta i_1 - \Delta i_2)/2$ (see Figure 3B). The series resistance in the conducting glass was checked using impedance spectroscopy (CH Instruments, model 660A) and a correction for the voltage decrease in the conducting glass was made: $\Delta U_{corr} = \Delta U - i_{film} \times R_{series}$. The resistance ($R$) of the TiO_2 film permeated with electrolyte was calculated as follows:

$$R = \frac{\Delta U_{corr}}{i_{film}}$$

2.5. Analysis of TiO_2 Film. The dimensions of the TiO_2 films (i.e., thickness (d), width (w), length (L), and gap length (l)) were measured by a profilometer (Dektak 3) after the conductivity experiments. The dimensions were typically $d = 7$ μm, $w = 1.5$ cm, $L = 0.5$ cm, and $l = 90$ μm. The thickness of the film across the gap was assumed to be the same as that beside the gap.

3. Results

3.1. Conductivity of TiO_2 Film Permeated with Electrolyte. Equilibrium currents at potentials ranging from −0.5 V to −1.0 V and −0.75 V to −1.25 V were registered for the TiO_2 films that were permeated with $LiCF_3SO_3$ and $CsClO_4$ electrolytes, respectively. The signal-to-noise ratio of the equilibrium currents was too low for accurate measurement at more-positive potentials. The conductivity (κ) was determined from the resistance (R), the gap length (l), and the cross-sectional area (A), thickness (d), and width (w) of the TiO_2 film using eq 1.

$$\kappa = \frac{1}{RA} = \frac{l}{Rwd} = \frac{l}{wd}\left(\frac{i_{film}}{\Delta U_{corr}}\right) \quad (1)$$

The potential dependence of the conductivity for the TiO_2 film immersed in the 500 mM $LiCF_3SO_3$ electrolyte is shown in Figure 4A. The conductivity increases strongly when more-negative potentials are applied. Figure 4B shows that this increase in conductivity is approximately exponential. When lower concentrations of $LiCF_3SO_3$ are used, the conductivity curves are slightly shifted toward more-negative potentials but are otherwise very similar. A further negative potential shift of the conductivity curve is observed when 10 mM $CsClO_4$ is used instead of 10 mM $LiCF_3SO_3$. A measurable conductivity was observed at approximately −0.75 V for the TiO_2 film that was permeated with 10 mM $CsClO_4$, which is a potential shift of −0.15 V, compared to that for the 10 mM $LiCF_3SO_3$ electrolyte. The addition of 500 mM 4TBP to the 500 mM $LiCF_3SO_3$ electrolyte led to a slight increase in conductivity between −0.6 V and −0.7 V and a decrease between −0.9 V and −1.0 V.

The resistivity ($\rho = \kappa^{-1}$) of the nanostructured TiO_2 film in 500 mM $LiCF_3SO_3$ at 25 °C was calculated to be between 45 Ω m and 0.01 Ω m in the potential range of −0.5 V to −1.0 V. By comparison, the resistivity of a typical insulator such as rubber is 5×10^{13} Ω m, whereas that of germanium (a semiconductor) is 0.46 Ω m and that of copper is 1.67×10^{-8} Ω m. In macroscopic single crystals of doped anatase TiO_2, a resistivity of 0.001 Ω m has been measured.[18]

The temperature (T) dependence of the conductivity in the nanostructured TiO_2 film permeated with electrolyte was studied. An increase of conductivity with increasing temperature is observed. An Arrhenius plot of the conductivity at −0.7 V is

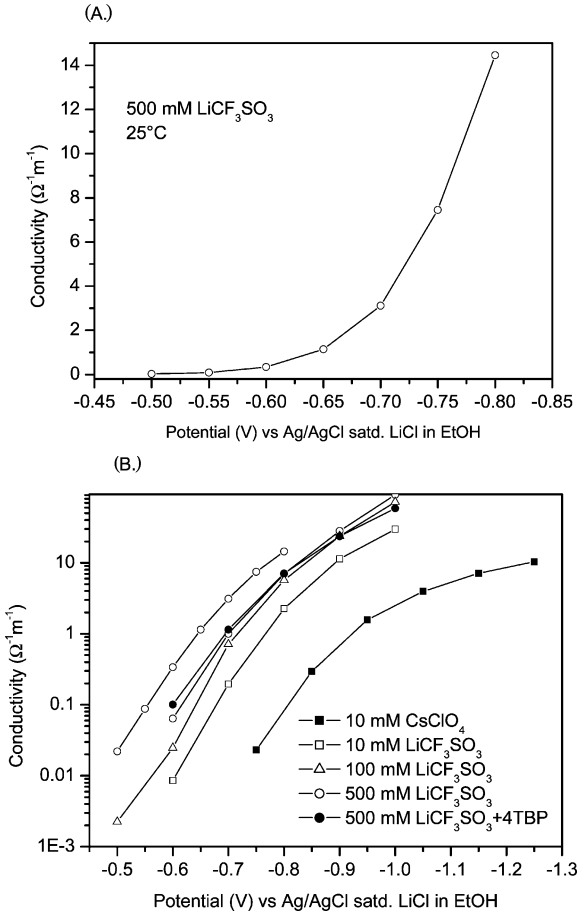

Figure 4. (A) Conductivity of the nanostructured TiO_2 film permeated with 500 mM $LiCF_3SO_3$ in propylene carbonate at 25 °C, as a function of potential. (B) Conductivity (logarithmic scale) versus potential for all electrolytes (10 mM, 100 mM, and 500 mM $LiCF_3SO_3$; 500 mM $LiCF_3SO_3$ and 4-*tert*-butylpyridine (4TBP); and 10 mM $CsClO_4$ in propylene carbonate).

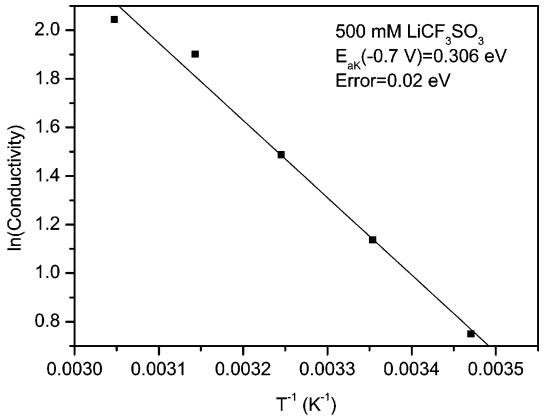

Figure 5. Arrhenius plot of electron conductivity in the nanostructured TiO_2 film permeated with the electrolyte 500 mM $LiCF_3SO_3$ in propylene carbonate at the applied potentials of −0.7 V and −0.71 V versus Ag/AgCl with saturated LiCl in ethanol.

shown in Figure 5. The activation energy of the electron conduction ($E_{a\kappa}$) at −0.7 V for a TiO_2 film permeated with 500 mM $LiCF_3SO_3$ was calculated to 0.3 eV with the Arrhenius equation:

$$\ln \kappa = \ln B - \frac{E_{a\kappa}}{kT} \qquad (2)$$

where B is a pre-exponential factor and k is the Boltzmann

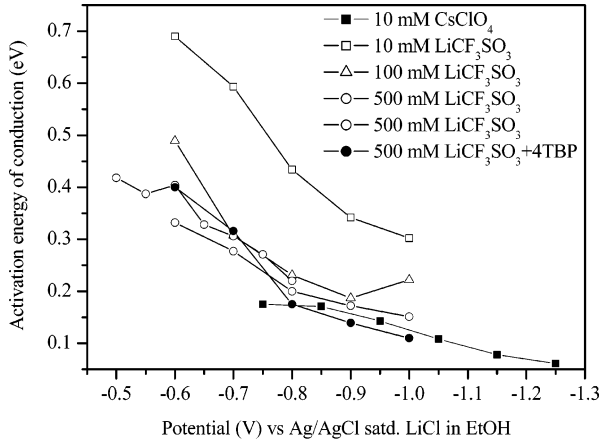

Figure 6. Activation energy of electron conduction ($E_{a\kappa}$) in the nanostructured TiO_2 film permeated with the electrolytes (10 mM, 100 mM, and 500 mM $LiCF_3SO_3$; 500 mM $LiCF_3SO_3$ and 4-*tert*-butylpyridine (4TBP); and 10 mM $CsClO_4$ in propylene carbonate), as a function of potential.

constant. The activation energy of conduction, as a function of potential, is shown in Figure 6 for the different electrolytes. The activation energy decreased almost linearly with more-negative applied potential. Furthermore, an increase in the $LiCF_3SO_3$ concentration led to a decrease in activation energy. The addition of 4TBP did not significantly change the activation energy of conduction. The activation energies were 0.4−0.15 eV for the electrolyte 500 mM $LiCF_3SO_3$ in the potential range of −0.5 V to −1.0 V. By comparison, the activation energy in a large single crystal of TiO_2 (anatase), without an electrolyte, was determined to be 0.0042 eV.[18] The activation energies in the 10 mM $CsClO_4$ the electrolyte were significantly lower than those in the 10 mM $LiCF_3SO_3$.

3.2. Electron Accumulation in TiO_2 Film. In Figure 7A, the number of electrons per TiO_2 particle is shown as a function of potential and electrolyte concentration. The electron concentration was calculated from the accumulated charge in the TiO_2 film (Q_{acc}) and the number of TiO_2 particles in the entire film. The number of TiO_2 particles ($\sim 2.5 \times 10^{14}$ cm^{-2}) was approximated from the dimensions of the film (w, d, L), a porosity of 50%, and a mean particle diameter of 13 nm. The number of electrons per particle increased with more-negative potential and increased concentration of $LiCF_3SO_3$. For the 10 mM $CsClO_4$ the number of electrons per particle also increased with more-negative potential; however, the increase was not as steep as that for the 10 mM $LiCF_3SO_3$. The number of electrons per TiO_2 particle was 13−423 in the potential range of −0.6 V and −1.0 V for the 500 mM $LiCF_3SO_3$.

The electrons in the TiO_2 particles are possibly occupying surface Ti atoms. Transmission electron microscopy (TEM) studies on nanostructured TiO_2 (anatase) electrodes have shown that the exposed planes are mainly (101) and (010).[22] The density of surface Ti atoms on these planes is calculated to be 5.16×10^{14} cm^{-2} and 5.55×10^{14} cm^{-2}, respectively. For a TiO_2 particle with a radius of 6.5 nm, the number of surface Ti atoms is ∼2800. The electron coverage of surface Ti atoms is also shown in Figure 7A. Assuming that the electrons are located at the surface, ∼15% of the surface Ti atoms are occupied with an electron at −1.0 V for the 500 mM $LiCF_3SO_3$, 5% for the 10 mM $LiCF_3SO_3$ and 2% for the 10 mM $CsClO_4$.

Linear graphs are obtained when $\ln(n_{part})$ is plotted versus the potential (Figure 7B), where n_{part} is the number of electrons per TiO_2 particle. The slopes and intercepts (at 0 V) of the graphs varied with the size and concentration of the cation but

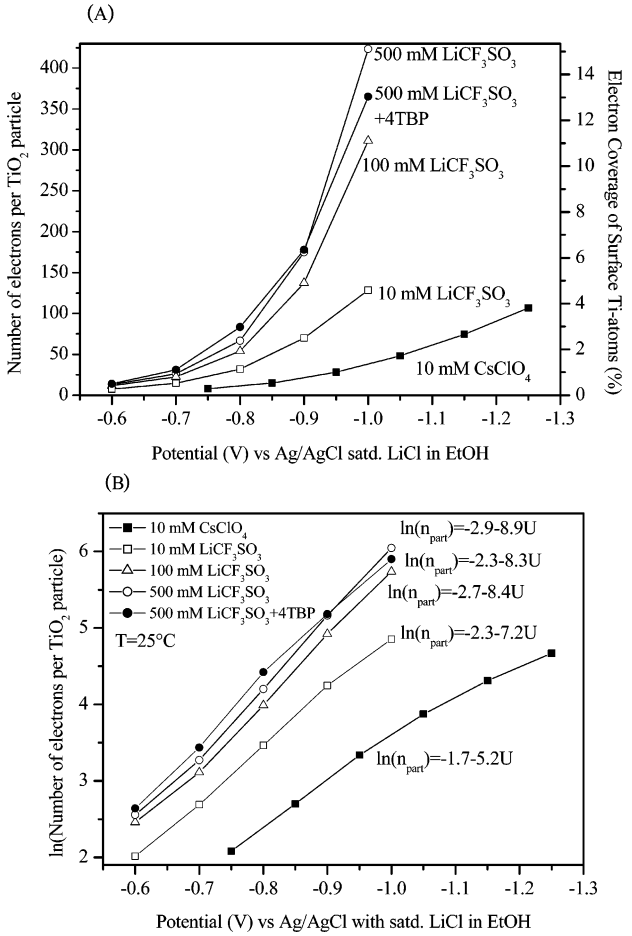

Figure 7. (A) Number of electrons per TiO_2 particle (n_{part}) and the electron coverage of surface Ti atoms of the nanostructured TiO_2 film permeated with electrolytes (10 mM, 100 mM, and 500 mM $LiCF_3SO_3$; 500 mM $LiCF_3SO_3$ and 4-*tert*-butylpyridine (4TBP); and 10mM $CsClO_4$ in propylene carbonate at 25 °C, as a function of potential. (B) Graphs of $\ln(n_{part})$ as a function of potential for the electrolytes (10 mM, 100 mM, and 500 mM $LiCF_3SO_3$; 500 mM $LiCF_3SO_3$ and 4TBP; and 10 mM $CsClO_4$ in propylene carbonate at 25 °C).

not significantly with temperature. The charge injected into the TiO_2 increases exponentially as the applied negative potential increases, with an exponent of $\sim 9\ V^{-1}$ for the 500 mM $LiCF_3SO_3$ and $5\ V^{-1}$ for the 10 mM $CsClO_4$.

The temperature dependence of electron accumulation was also studied. An increase of the temperature leads to an increase in the accumulated charge at a given potential. Activation energies for electron accumulation in the nanostructured TiO_2 (E_{aQ}) were obtained from Arrhenius plots ($\ln(n_{part})$ vs T^{-1}). The results are shown in Figure 8. For the Li^+-based electrolytes, E_{aQ} seems to increase with more-negative applied potentials, leveling off at approximately -0.7 V. Reducing the concentration of Li^+ cations gives an increase in E_{aQ}. In the Cs^+-based electrolyte, E_{aQ} is smaller and more constant.

3.3. Effective Mobility and Diffusion Coefficient of Electrons. In Figure 9, the conductivity is plotted as a function of the number of electrons per TiO_2 particle for the 500 mM $LiCF_3SO_3$. For all electrolytes, two regions can be distinguished. In the first region (0−20 electrons per TiO_2 particle), the conductivity increases in a nonlinear way, relative to the accumulated electrons in the particle. In the second region (>20 electrons per TiO_2 particle), the conductivity increases linearly as the number of electrons per TiO_2 particle increases.

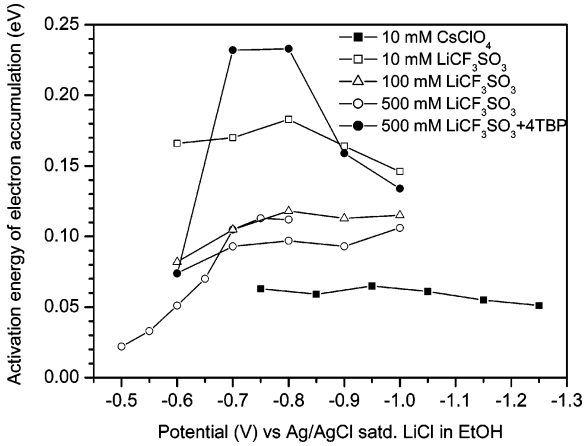

Figure 8. Activation energy of electron accumulation (E_{aQ}) in the nanostructured TiO_2 film permeated with the electrolytes (10 mM, 100 mM, and 500 mM $LiCF_3SO_3$; 500 mM $LiCF_3SO_3$ and 4-*tert*-butylpyridine (4TBP); and 10 mM $CsClO_4$ in propylene carbonate), as a function of potential.

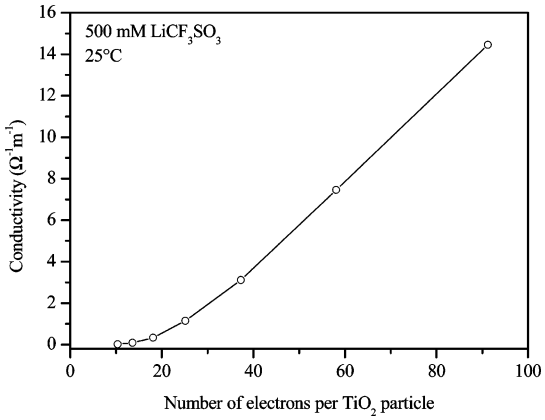

Figure 9. Conductivity (κ) of the nanostructured TiO_2 film permeated with 500 mM $LiCF_3SO_3$ in propylene carbonate, as a function of the number of electrons per TiO_2 particle at 25 °C.

We can calculate an effective mobility for electrons in the nanostructured TiO_2 electrode (μ_{eff}) from the measured conductivity (κ) and the total density of electrons in the TiO_2 (n) using eq 3:

$$\kappa = q_e n \mu_{eff} \tag{3}$$

where q_e is the electronic charge. The effective mobility is proportional to the slope of the graph of conductivity versus the number of electrons per particle (see Figure 9). In the linear region, μ_{eff} is independent of the number of electrons per TiO_2 particle and, therefore, is also independent of the applied potential. An effective mobility of $150 \times 10^{-4}\ cm^2\ V^{-1}\ s^{-1}$ was calculated from the slope of the graph in the linear region (500 mM $LiCF_3SO_3$). Table 1 lists the μ_{eff} values that were determined in this manner for the different electrolytes. The concentration of the electrolyte seems to have a weak effect on the mobility. A strong effect of the nature of the electrolyte (10 mM $LiCF_3SO_3$ vs 10 mM $CsClO_4$) was observed: the $CsClO_4$ electrolyte gives a significantly lower effective mobility of electrons in the nanostructured TiO_2. Also, the addition of 4TBP led to a reduction in mobility. The effective mobility varied slightly with temperature for the $LiCF_3SO_3$ electrolytes. Activation energies of the effective electron mobility were determined using the Arrhenius equation and are listed in Table 1. Although μ_{eff} has an activation energy of $\sim$0.1 eV in the $LiCF_3SO_3$

TABLE 1: Effective Electron Mobility (μ_{eff}), Effective Diffusion Coefficient (D_{eff}) of Electrons, and Activation Energy of the Mobility ($E_{a\mu}$) in Region 2 in the Nanostructured TiO_2 Film Permeated with Electrolytes (10 mM, 100 mM, and 500 mM $LiCF_3SO_3$; 500 mM $LiCF_3SO_3$ and 500 mM 4-*tert*-butylpyridine (4TBP); and 10 mM $CsClO_4$ in Propylene Carbonate at 25 °C)

electrolyte	μ_{eff}[a] (10^{-4} cm^2 V^{-1} s^{-1})	D_{eff} (10^{-5} cm^2 s^{-1})	$E_{a\mu}$[a] (eV)
10 mM $LiCF_3SO_3$	190 (16)	50	0.16 (0.03)
100 mM $LiCF_3SO_3$	180 (10)	45	0.11 (0.01)
500 mM $LiCF_3SO_3$	160 (8)	40	0.07 (0.01)
500 mM $LiCF_3SO_3$ and 500 mM 4TBP	130 (5)	30	−0.01 (0.01)
10 mM $CsClO_4$	80 (2)	20	0.01 (0.01)

[a] Error values are shown in brackets.

TABLE 2: Effective Electron Mobility (μ_{eff}) and Effective Diffusion Coefficient (D_{eff}) of Electrons at 25 °C and Activation Energies of Mobility ($E_{a\mu}$), Electron Accumulation (E_{aQ}), and Conduction ($E_{a\kappa}$) in Region 1 for 500 mM $LiCF_3SO_3$ at Different Potentials versus Ag/AgCl with Saturated LiCl in Ethanol

potential (V)	μ_{eff} ($\times 10^{-4}$ cm^2 V^{-1}s^{-1})	D_{eff} ($\times 10^{-5}$ cm^2/s)	$E_{a\mu}$[a] (eV)	E_{aQ}[a] (eV)	$E_{a\kappa}$[a] (eV)
−0.6	78	20	0.28 (0.06)	0.05 (0.01)	0.40 (0.03)
−0.55	19	5	0.28 (0.07)	0.03 (0.01)	0.39 (0.04)
−0.5	7	2	0.31 (0.08)	0.02 (0.01)	0.42 (0.07)

[a] Error values are shown in brackets.

electrolytes, it seems to be activationless in the $LiCF_3SO_3$/4TBP and $CsClO_4$ electrolytes.

The effective diffusion coefficient (D_{eff}) for electrons was calculated using the Einstein relation:

$$D_{eff} = \frac{\mu_{eff} kT}{q_e} \tag{4}$$

Consequently, the effective diffusion coefficient of the electrons is independent of the number of electrons per TiO_2 particle and the applied potential in region 2, but varies with the type and concentration of the electrolyte ions. The effective diffusion coefficient of electrons is 2×10^{-4}−5×10^{-4} cm^2/s (see Table 1).

4. Discussion

In conventional *n*-type semiconductor materials, the electronic conduction is given by

$$\kappa = q_e n_C \mu_C \tag{5}$$

where n_C and μ_C are the concentration and mobility of electrons in the conduction band, respectively. The mobility usually is only weakly activated, if at all. The energy difference between the lower edge of the conduction band (E_C) and the Fermi level (E_F) determines the electron concentration. If $E_C - E_F \gg kT$, then

$$n_C = N_C \exp\left(-\frac{E_C - E_F}{kT}\right) \tag{6}$$

where N_C is the effective density of conduction band states. In the bulk of the semiconductor, n_C and E_F are constant; they are determined by the temperature and the concentration and type of the donor impurities. The situation is clearly different in nanostructured semiconductor electrodes. They are usually not intentionally doped and n_C and E_F are directly controlled by the externally applied potential. Furthermore, the electrolyte in the pores of the electrode has a significant role in the electron conduction in the nanostructured electrode. Although it is convenient to measure and discuss conductivities in nanostructured TiO_2, one should remember that the electron transport is not driven by an electric field. The applied potential difference leads to a difference in electron concentration between the two sides of the working electrode, which results in a diffusion-driven current.

Using a combination of chronoamperometry and conductivity measurements, we have determined that the electronic conductivity of nanostructured TiO_2 immersed in an electrolyte can be divided in two distinct regions: In region 1, the conductivity changes in a nonlinear fashion with the charge, whereas a linear relation is observed in region 2. Also, the activation energies of conductivity, mobility, and charge accumulation differ significantly between regions 1 and 2. We will discuss the two regions separately below.

4.1. Region 1: Nonlinear Increase of Conductivity with Charge. Region 1 (up to 20 electrons per TiO_2 particle, potential down to −0.6 V (for 0.5 M $LiCF_3SO_3$)) corresponds roughly to the region wherein the well-known dye-sensitized nanostructured solar cell operates. The relevant potentials for the charge transport in the TiO_2 film in the solar cell are between +0.2 V and −0.5 V vs Ag/AgCl (saturated LiCl in ethanol), whereas the redox potential of the dye $[Ru(dcbpyH_2)_2(NCS)_2]$ is +0.95 V[24] and that of the redox couple I^-/I_3^- is +0.19 V. The sensitivity of our electrochemical methods is limited in this region; therefore, the results are more uncertain than those in region 2.

In region 1, the conductivity shows a nonlinear dependence on the electron concentration, implying that the effective mobility changes as a function of charge. An estimate for the mobility was made from the slope of a fitted exponential function through the data points in the conductivity versus the electron concentration plot. The values of the effective electron mobility are in the range of 7×10^{-4}−78×10^{-4} cm^2 V^{-1} s^{-1} (see Table 2). The corresponding effective diffusion coefficients are in the range of 2×10^{-5}−20×10^{-5} cm^2/s. These values correspond well with those measured in nanostructured dye-sensitized solar cells under strong illumination.[5,8] From temperature-dependent studies, the activation energy of the effective electron mobility ($E_{a\mu}$) was determined to be 0.3 eV, independent of the applied potential. The activation energy of electron accumulation (E_{aQ}) was ∼0.02−0.05 eV in the potential range of −0.5 V to −0.6 V.

In region 1, the effective mobility (diffusion coefficient) in the nanostructured TiO_2 changes with the electron concentration. It has a large activation energy of 0.3 eV and it is very small in comparison with that of an anatase TiO_2 single crystal. These

observations exclude pure band conduction (eq 5) as a mechanism for charge transport. Similar observations have been made in dye-sensitized solar cells. The most frequently used explanation is that a large fraction of the electrons is trapped in states below the conduction band. These electrons are immobile unless they are thermally excited to the conduction band. The measured μ_{eff} is equal to $(n_C/n)\mu_C$ (eq 5 becomes eq 3). Depending of the distribution of the trap states (in energy and density), different transport characteristics can be obtained. An exponential distribution is proposed in several studies. This would also fit our results in region 1, to some extent. The nonlinear increase of conductivity with charge might follow a power-law dependence, as follows from an exponential trap distribution (see Appendix A). The negligible change in accumulated charge with temperature ($E_{aQ} \approx 0$) also agrees with the presence of a great number of localized states below the conduction band edge. The activation energy for the effective mobility is expected to be $E_C - E_F$, which is the thermal energy needed for detrapping of electrons from the highest filled trap states to the conduction band. In our study, however, $E_{a\mu}$ seems to be constant (0.3 eV), independent of the applied potential, which is in contradiction with the trapping/detrapping model with an exponential trap distribution (see Appendix A).

An alternative electron transport mechanism is hopping. In this case, the conduction band is not involved: electrons trapped in localized states jump to adjacent states. The localized states could be, for instance, the Ti atoms at the semiconductor/electrolyte interface (see Appendix B). This would explain the observed electrolyte dependence. Hopping transport is generally characterized by low mobilities with high activation energies. In the model proposed in Appendix B, where all hopping sites are equivalent, a linear relation between conductivity and charge is predicted, in contrast to the observations in region 1. Therefore, this hopping model is not valid in region 1. Other, more-complex, hopping models in which a certain distribution of hopping states over energy and/or distance is assumed might account for the electron transport. However, a more-detailed analysis lies outside the scope of this paper.

In summary, the trapping/detrapping model can explain the electron transport in nanostructured TiO_2 that has been permeated with electrolytes in region 1 rather well: the low mobility, the weak temperature dependence of electron accumulation, and the high activation energy for the effective mobility can be explained. However, the constant value of $E_{a\mu}$ with applied potential is not predicted in this model.

4.2. Region 2: Linear Increase of Conductivity with Charge. Region 2 (>20 electrons per particle, potentials more negative than −0.6 V (0.5 M $LiCF_3SO_3$)) is characterized by a linear relation between electron conductivity and accumulated charge in the nanostructured TiO_2 electrode, resulting in a constant effective mobility. This agrees with electron transport in the conduction band as described by eq 5. However, note that the obtained mobilities are ∼2 orders of magnitude lower than those found in single-crystalline TiO_2 (anatase), and that the mobility is dependent on the electrolyte. These observations suggest a fundamental difference between conventional band conduction in a semiconductor and conduction in a nanostructured semiconductor that is permeated with an electrolyte.

Based on the finding that the effective mobility is independent of accumulated charge and applied potential, we propose that electrons in the conduction band are responsible for charge transport in region 2. Spectroelectrochemical studies in this region have shown that the accumulated electrons give a monotonic increase of the optical absorption with wavelength, suggesting that they are (mainly) delocalized.[13,20] In the present study, a small activation energy is observed for the mobility, which may agree with band conduction in the case of polarons.

The activation energy for conductivity is strongly dependent on the applied potential (see Figure 6). Equation 3 shows that $E_{a\kappa}$ is the sum of the activation energies of charge accumulation and effective mobility. Because $E_{a\mu}$ is constant in region 2, this implies that E_{aQ} should be strongly dependent on the applied potential. However, Figure 8 shows that E_{aQ} is relatively constant in region 2. The reason for these apparently conflicting results is not clear and will be addressed in future studies.

Interestingly, the activation energy of the effective electron mobility is dependent on the electrolyte (see Table 1). Although the activation energy is ∼0.1 V for the $LiCF_3SO_3$ electrolytes, it is almost zero for the electrolytes with $CsClO_4$ and $LiCF_3SO_3$ + 4TBP. A possible explanation is that there is an electrostatic attraction between the electron and the charge-compensating cation in the electrolyte. Because the Li^+ ion (without solvation shell) is smaller than the Cs^+ ion, it can approach the electron in the TiO_2 more closely. The resulting electrostatic binding energy possibly corresponds to the activation energy for the mobility. Li^+ and 4TBP are believed to form a complex[25] and, because $(Li\text{-}4TBP)^+$ is a large ion, there will be only weak interactions with the electron.

The variation of the diffusion coefficient, relative to the Li^+ concentration in region 2, i.e., a small decrease with increasing cation concentration, does not agree with the trend found in other studies.[4,15,26] In these studies, laser-pulse-induced photocurrent measurements were used and an increase of the diffusion coefficient with increased Li^+ concentration was observed. The difference in experimental conditions can possibly explain the different trends. In the present study, conductivity is measured in a steady-state situation. The accumulated electrons in the nanostructured TiO_2 electrode are charge-compensated by additional cations in the pores of the nanostructured electrode that have entered from the bulk electrolyte, so that the cation concentration is larger in the pores than in the bulk electrolyte. In the laser-pulse experiments, charge-compensation cations must enter pores of the nanostructured electrode upon electron generation. This can possibly give an addition delay for the electron transport, which will seem to make the electron diffusion coefficient slower with lower electrolyte concentrations.

Can the results obtained in region 2 also be explained using a trapping/detrapping or hopping model? In the trapping/detrapping model, the linear dependence of conductivity with charge can be explained by assuming a certain trap level located below E_C and above E_F (see Appendix A). The ratio of the conduction band electrons to trapped electrons is then fixed; it is determined by the energy difference between E_C and the trap level E_T. The activation energy for the effective mobility would then be $E_C - E_T$. The effect of these traps would be that electron transport is slowed and that the effective mobility becomes activated. Based on the findings in Table 1, such a model seems reasonable, because the trap depth could be determined by the cation in the electrolyte: 0.1 eV for Li^+ and 0 eV (no trapping) for Cs^+. The measured values of μ_{eff} are in contradiction with this model, because the mobility in Li electrolytes is higher than that in the Cs electrolyte.

A linear dependence of conductivity with charge follows from the hopping model proposed in Appendix B, in accordance with the observations in region 2. An activation energy for the mobility is expected in the hopping model. For the Cs^+ and $(Li\text{-}4TBP)^+$ electrolytes, however, no activation was observed,

whereas the measured effective mobility was less than that in Li^+ electrolytes, which seems to contradict this hopping model.

4.3. Electron Accumulation and Conduction Band Edge Position. The curves of both the conductivity versus potential and the accumulated charge versus potential show a marked effect of the concentration of the $LiCF_3SO_3$ electrolyte. The onset for electron accumulation shifts to more-positive potentials with increasing electrolyte concentration (see Figure 7). Similar observations have been made in spectroelectrochemical studies of nanostructured TiO_2 in nonprotic electrolytes.[27] The propylene carbonate used in this study is also a nonprotic solvent, so that similar behavior can be expected. The explanation for the observed shifts is that the position of the conduction band edge is dependent on the amount of cations adsorbed at the inner Helmholtz double layer of the TiO_2/electrolyte interface. The degree of specific adsorption of the cation is dependent on the concentration in the electrolyte and on the nature of the cation. In contrast to the Li^+ cation, the Cs^+ cation has a low affinity for the TiO_2 surface, resulting in a more-negative position of E_C.

An accumulation of electrons in the nanostructured TiO_2 electrode will lead to a shift of the conduction band edge energy. If $E_C(0)$ is the conduction band edge without accumulated electrons, then a charge Q accumulated in the nanostructured electrode causes the level of the conduction band edge to shift to $E_C(Q)$ as follows:

$$E_C(Q) = E_C(0) + \frac{qQ}{\mathrm{rf}C_H} \tag{7}$$

where rf is the roughness factor of the electrode and C_H is the Helmholtz capacitance. The shift is caused by the additional charge in the Helmholtz layer, resulting in an additional voltage difference across this layer. In practical terms, it means that, on application of a negative potential to the nanostructured electrode, the conduction band edge potential shifts to more-negative potentials, depending on the charge that accumulates in the electrode. Assuming a roughness factor of rf = 600 for our electrode and $C_H = 10^{-5}$ F/cm^2, it is calculated that the conduction band edge would shift 0.62 V in the negative direction for the applied potential of −0.8 V (0.5 M $LiCF_3SO_3$, 25 °C, Q_{acc}= 3.7 mC/cm^2). This seems to be an unrealistic result. It is likely that the surface charge of the TiO_2 due to absorbed ions changes when electrons are accumulated, resulting in a much smaller shift of the conduction band edge.

In region 2, the accumulated electrons seem to be conduction band electrons. Equation 6 predicts that the number of conduction band electrons increases exponentially as the value of the term $E_C - E_F$ decreases. In our experiment, the position of the Fermi level is controlled by means of a potentiostat. Therefore, one can expect that the charge in the nanostructured TiO_2 electrode will increase exponentially with applied negative potential. This is confirmed in Figure 7B. However, the exponents that are determined are much lower than the 38.9 V^{-1} that follows from eq 6. They were determined to range from 8.9 V^{-1} to 5.2 V^{-1} for the 500 mM $LiCF_3SO_3$ and the 10 mM $CsClO_4$, respectively. Part of the difference may result from the shift of E_C with accumulated charge. If the charging of the Helmholtz layer would dominate, however, a linear relation between charge and potential should be found. The low exponents have been attributed to an exponential tail of trap states.[12] However, this observation contradicts our conductivity results. Instead, we see the low exponents as a characteristic of nanostructured semiconductor electrodes that is not fully understood.

5. Conclusion

We have developed a technique from which activation energies of conduction, electron accumulation, and mobility in nanostructured semiconductor electrodes can be determined. From the relationship between conductivity and electron concentration, two regions were distinguished. In the first region (∼1−20 electrons per TiO_2 particle), which best resembles the region where the nanostructured dye-sensitized solar cell operates, the results can be fitted, to some extent, with a trapping/detrapping model for charge transport, but not with a conduction band model. The effective electron mobility is dependent on the electron concentration and values in the range of 7×10^{-4}−78×10^{-4} cm^2 V^{-1} s^{-1} have been determined. For the second region (>20 electrons per TiO_2 particle), charge transport by electrons in the conduction band seems to be the most applicable model. The effective electron mobility is independent of electron concentration and was calculated to be $\sim 150 \times 10^{-4}$ cm^2 V^{-1} s^{-1}.

Appendix A: Trapping/Detrapping Models

Many publications in the field of nanostructured dye-sensitized solar cells suggest the presence of electronic states (traps) with energies located below the conduction band. The presence of these states does not change the validity of eqs 6 and 7. However, the total density of electrons will be larger in the case of trapping at a given E_F level, because it is the sum of the conduction band electrons (n_C) and the trapped electrons (n_T). The distribution of the traps in the band gap determines the electron transport characteristics of the nanostructured semiconductor.

In the case of a single trap level E_T, the following relation (analogous to eq 6) can be derived:

$$n_T = N_T \exp\left(-\frac{E_T - E_F}{kT}\right) \tag{A1}$$

where N_T is the effective density of trap states (eq A1 is valid if $E_T - E_F \gg kT$). Combination with eq 6 gives

$$\frac{n_C}{n_T} = \frac{N_C}{N_T} \exp\left(-\frac{E_C - E_T}{kT}\right) \tag{A2}$$

From eq A2, it follows that n_C is a constant fraction of the total number of electrons ($n = n_C + n_T$). This means that a single trap level can give an overall reduction of the effective electron mobility but cannot explain a change in mobility with n. The activation energy of μ_{eff} will be $E_C - E_T$.

An exponential distribution of traps is more commonly assumed in nanostructured semiconductor electrodes. Van de Lagemaat and Frank derived the following expression for this case:[7]

$$n_C \propto {n_T}^{m/kT} \approx n^{m/kT} \tag{A3}$$

where m is the slope of the trap distribution curve that is defined by $N_T(E) = N_{T0} \exp[(E - E_0)/m]$, in which N_{T0} is the trap density at an energy E_0. The parameters n_C and μ_{eff} will show a power-law dependence, with respect to n. The activation energy for μ_{eff} will be approximately equal to the energy difference of the highest filled traps and the conduction band ($\sim(E_C - E_F)$) and will be dependent strongly on the applied potential and n.

Appendix B: A Hopping Model

Hopping of electrons between localized state has been suggested as a possible transport mechanism in dye-sensitized

nanostructured solar cells; however, to our knowledge, it has not been analyzed in detail yet. Here, we propose a simple hopping model, in which we assume that electron transport occurs between adjacent redox centers at the surface of the nanostructured TiO_2 electrode. These redox centers are surface Ti atoms that have a valency of 4+ when they are empty, or 3+ when they are occupied by an electron. Assuming that all the hopping sites are equivalent, the conductivity can be described in the following way:

$$\kappa \propto q_e n(N-n)\mu_{hop} \tag{B1}$$

where n is the density of sites occupied by electrons (Ti_s^{3+}) and N is the total density of sites (all surface Ti atoms). The parameter μ_{hop} is the hopping mobility, which has an activation energy E_{hop}. The potential dependence of n is given by the Nernst equation, which can be rewritten as follows:

$$\frac{[Ti_s^{3+}]}{[Ti_s^{4+}]} = \frac{n}{N-n} = \exp\left(-\frac{E^{0'}-E_F}{kT}\right) \tag{B2}$$

where $E^{0'}$ is the formal redox energy of the Ti_s^{3+}/Ti_s^{4+} redox couple. $E^{0'}$ will be dependent on the electrolyte used (for instance, on the cations present).

The described hopping model has the following characteristics:

(1) From eq B1, it follows that the conductivity increases linearly with n, for $n \ll N$. This is in disagreement with the results found in region 1 of this work and the results from the transport measurements of dye-sensitized solar cells. It agrees with the results of region 2. Calculation shows that $n \ll N$ is valid even in region 2 (see Figure 7A, right-hand axis).

(2) The charge in the nanostructured electrode should increase exponentially with applied negative potential with an exponent of 38.9 V^{-1} at room temperature, when $E_F \ll E^{0'}$ (see eq B2). Experimentally, the charge increases exponentially with a much lower exponent (8.9 for 0.5 M Li^+; see Figure 7B). Such a decrease in exponent is not uncommon in surface-redox reactions, because of interaction between the surface sites.

(3) The activation energy of the mobility is constant and nonzero (E_{hop}). This is in agreement with the experiments in region 2.

(4) The activation energy for electrode charging at a given potential is equal to ($E^{0'} - E_F$), as follows from eq B2.

Acknowledgment. The authors would like to thank Sven Södergen and Henrik Lindström for initializing conductivity experiments and useful discussions. This work has been supported by the Swedish National Energy Administration (Energimyndigheten), the Swedish Foundation for Strategic Environmental Research (MISTRA), and the PSO-project (under ELTRA Project No. 3629 (Denmark)).

References and Notes

(1) O'Regan, B.; M. Grätzel. *Nature (London)* **1991**, *353*, 737.
(2) Könenkamp, R. *Phys. Rev. B* **2000**, *61*, 11057.
(3) Bisquert, J.; Cahen, D.; Hodes, G.; Rühle, S.; Zaban, A. *J. Phys. Chem. B* **2004**, *108*, 8106−8118.
(4) Solbrand, A.; Lindström, H.; Rensmo, H.; Hagfeldt, A.; Lindquist, S.-E. *J. Phys. Chem. B* **1997**, *101*, 2514.
(5) Peter, L. M.; Wijayantha, K. G. U. *Electrochim. Acta* **2000**, *45*, 4543.
(6) van de Lagemaat, J.; Park, N.-G.; Frank, A. J. *J. Phys. Chem. B* **2000**, *104*, 2044.
(7) van de Lagemaat, J.; Frank, A. J. *J. Phys. Chem. B* **2000**, *104*, 4292.
(8) van der Zanden, B.; Goossens, A. *J. Phys. Chem. B* **2000**, *104*, 7171.
(9) Franco, G.; Gehring, J.; Peter, L. M.; Ponomarev, E. A.; Uhlendorf, I. *J. Phys. Chem. B* **1999**, *103*, 692.
(10) de Jongh, P. E.; Vanmaekelbergh, D. *J. Phys. Chem. B* **1997**, *101*, 2716.
(11) Fabregat-Santiago, F.; Garcia-Belmonte, G.; Bisquert, J.; Zaban, A.; Salvador, P. *J. Phys. Chem. B* **2002**, *106*, 334.
(12) Fabregat-Santiago, F.; Mora-Seró, I.; Garcia-Belmonte, G.; Bisquert, J. *J. Phys. Chem. B* **2003**, *107*, 758.
(13) Boschloo, G.; Fitzmaurice, D. *J. Phys. Chem. B* **1999**, *103*, 2228.
(14) Wang, H.; He, J.; Boschloo, G.; Lindström, H.; Hagfeldt, A.; Lindquist, S.-E. *J. Phys. Chem. B* **2001**, *105*, 2529.
(15) Nakade, S.; Kambe, S.; Kitamura, T.; Wada, Y.; Yanagida, S. *J. Phys. Chem. B* **2001**, *105*, 9150.
(16) Beermann, N.; Boschloo, G.; Hagfeldt, A. *J. Photochem. Photobiol. A: Chem.* **2002**, *152*, 213.
(17) Duffy, N. W.; Peter, L. M.; Rajapakse, R. M. G.; Wijayantha, K. G. U. *J. Phys. Chem. B* **2000**, *104*, 8916.
(18) Forro, L.; Chauvet, O.; Emin, D.; Zuppiroli, L.; Berger, H.; Lévy, F. *J. Appl. Phys.* **1994**, *75*, 633.
(19) Meulenkamp, E. A. *J. Phys. Chem. B* **1999**, *103*, 7831.
(20) van de Krol, R.; Goossens, A.; Meulenkamp, E. A. *J. Appl. Phys.* **2001**, *90*, 2235.
(21) Kittlesen, G. P.; White, H. S.; Wrighton, M. S. *J. Am. Chem. Soc.* **1984**, *106*, 7389.
(22) Shklover, V.; Nazeeruddin, M.-K.; Zakeeruddin, S. M.; Barbé, C.; Kay, A.; Haibach, T.; Steurer, W.; Hermann, R.; Nissen, H.-U.; Grätzel, M. *Chem. Mater.* **1997**, *9*, 430.
(23) Cox, P. A. *Transition Metal Oxides: An Introduction to Their Electronic Structure and Properties*; Oxford University Press: New York, 1992.
(24) Nazeeruddin, M. K.; Kay, A.; Rodicio, I.; Humphry-Baker, R.; Müller, E.; Liska, P.; Vlachopoulos, N.; Grätzel, M. *J. Am. Chem. Soc.* **1993**, *115*, 6382.
(25) Greijer Agrell, H.; Lindgren, J.; Hagfeldt, A. *J. Photochem. Photobiol. A: Chem.* **2004**, *164* (1−3), 23−27.
(26) Kambe, S.; Nakade, S.; Kitamura, T.; Wada, Y.; Yanagida, S. *J. Phys. Chem. B* **2002**, *106*, 2967.
(27) Redmond, G.; Fitzmaurice, D. *J. Phys. Chem. B* **1993**, *97*, 1426.